Simulation of ENSO with a Global Atmospheric GCM Coupled to a High-Resolution, Tropical Pacific Ocean GCM

S. G. H. PHILANDER, R. C. PACANOWSKI, N.-C. LAU, AND M. J. NATH

Geophysical Fluid Dynamics Laboratory/NOAA, Princeton University, Princeton, New Jersey

(Manuscript received 22 October 1990, in final form 10 September 1991)

ABSTRACT

A global atmospheric general circulation model (GCM) coupled to an oceanic GCM that is dynamically active only in the tropical Pacific simulates variability over a broad spectrum of frequencies even though the forcing, the annual mean incoming solar radiation, is steady. Of special interest is the simulation of a realistically irregular Southern Oscillation between warm El Niño and cold La Niña states. Its time scale is on the order of 5 years. The spatial structure is strikingly different in the eastern and western halves of the ocean basin. Sea surface temperature changes have their largest amplitude in the central and eastern tropical Pacific, but the low-frequency zonal wind fluctuations are displaced westward and are large over the western half of the basin. These zonal wind anomalies are essentially confined to the band of latitudes 10°N to 10°S so that they form a jet and have considerable latitudinal shear. During El Niño the associated curl contributes to a pair of pronounced minima in thermocline depth, symmetrically about the equator in the west, near 8°N and 8°S. In the east, where the low-frequency wind forcing is at a minimum, the deepening of the thermocline in response to the winds in the west has a very different shape—an approximate Gaussian shape centered on the equator.

The low-frequency sea surface temperature and zonal wind anomalies wax and wane practically in place and in phase without significant zonal phase propagation. Thermocline depth variations have phase propagation; it is eastward at a speed near 15 cm s^{-1} along the equator in the western half of the basin and is westward off the equator. This phase propagation, a property of the oceanic response to the quasi-periodic winds that force currents and excite a host of waves with periods near 5 years, indicates that the ocean is not in equilibrium with the forcing. In other words, the ocean–atmosphere interactions that cause El Niño to develop at a certain time are countered and, in due course, reversed by the delayed response of the ocean to earlier winds. This "delayed oscillator" mechanism that sustains interannual oscillations in the model differs in its details from that previously discussed by Schopf and Suarez and others. The latter investigators invoke an explicit role for Kelvin and Rossby waves. These waves cannot be identified in the low-frequency fluctuations of this model, but they are energetic at relatively short periods and are of vital importance to a quasi-resonant oceanic mode with a period near 7 months that is excited in the model. The similarities and differences between the results of this simulation and those with other models, especially the one described in a companion paper, are discussed.

1. Introduction

It is possible to simulate the atmospheric aspects of the Southern Oscillation with a general circulation model (GCM) provided realistic sea surface temperatures are specified as a lower boundary condition (Lau 1985). It is also possible to simulate its oceanic aspects with a GCM of the ocean provided realistic surface boundary conditions, especially surface winds, are specified (Philander and Seigel 1985). This paper describes a simulation of the El Niño/Southern Oscillation (ENSO) with coupled ocean–atmosphere GCMs so that each component provides the boundary conditions for the other. The atmospheric component is the global R15 model used by Lau (1985) in the study just mentioned. The oceanic component is a high-resolution model of the tropical Pacific, an improved version of the model used by Philander and Seigel (1985). Outside the tropical Pacific observed annual mean sea surface temperatures are specified. In the preceding companion paper, Lau et al. (1992) describe a simulation in which the same atmospheric component is coupled with a coarse-resolution, global oceanic GCM.

The coupled model simulates a broad spectrum of variability even though the forcing function, the annual mean solar radiation, is steady. (The seasonal cycle is absent from this model.) Some of the variability in the model is of atmospheric origin, some of the variability is of oceanic origin, and some of it depends on interactions between the ocean and atmosphere. Variability of the first type includes phenomena such as synoptic-scale weather, as well as the eastward-traveling equatorial disturbances that have intraseasonal time scales and that are prominent in the Indian and western Pacific oceans (Lau and Lau 1986). Such disturbances are observed in reality. An example of variability with

Corresponding author address: Dr. Ngar-Cheung Lau, Princeton University, Geophysical Fluid Dynamics Laboratory/NOAA, Forrestal Campus, US Route 1, P.O. Box 308, Princeton, NJ 08542.

a strictly oceanic origin is an instability associated with the latitudinal shear of the equatorial currents in the eastern Pacific during periods of intense southeast trades. The instability gives rise to westward-traveling waves with a period of approximately 3 weeks and a wavelength near 1000 km. This feature of the model agrees well with measurements (Philander et al. 1985). None of the relatively high-frequency oceanic and atmospheric disturbances mentioned thus far will receive much attention in this paper. The focus, rather, is on the low frequencies: interannual variations that are attributable to interactions between the ocean and atmosphere, and oceanic fluctuations with a period near 7 months that are associated with a quasi-resonant mode of the ocean. These simulated interannual fluctuations correspond to a Southern Oscillation between warm El Niño and cold La Niña states. High coherence between the low-frequency fluctuations of different oceanic and atmospheric parameters is the distinguishing feature of the Southern Oscillation. Conditions at the peak of a warm phase and at the peak of a cold phase are realistic, as realistic as in other coupled models that simulate the Southern Oscillation. The differences between this model, the one described by Lau et al. (1992), and the other coupled models lie in the manner in which the warm and cold phases develop. This paper will address such differences among various coupled models.

The paper is organized as follows. Section 2 describes the model, section 3 the time-mean conditions, section 4 the simulated Southern Oscillation, and section 5 the quasi-resonant mode of the ocean.

2. The model

The atmospheric R15 model is global, has nine layers in the vertical, and has a horizontal resolution of 4.5° latitude and 7.5° longitude [Lau et al. (1992) provides further details]. The oceanic model, a regional one for the tropical Pacific Ocean, has a domain, shown in Fig. 1a, that extends from 28°S to 50°N. The longitudinal resolution is a constant 100 km, but the latitudinal distance between grid points is 33 km between 10°S and 10°N and increases gradually poleward of this region. The spacing at 25°N is 200 km. The flat-bottom ocean is 4000 m deep. There are 27 levels in the vertical; the upper 100 m has a resolution of 10 m. The vertical mixing coefficients are Richardson number–dependent as in the parameterization proposed by Pacanowski and Philander (1981). The coefficients of horizontal eddy viscosity and diffusivity are 2×10^3 m^2 s^{-1} equatorward of 10° latitude; farther poleward they increase in value, especially near the boundary walls along 28°S and 50°N where the value is almost an order of magnitude larger. This large value creates a buffer zone near the walls where the observed mean oceanic temperatures are specified as a function of depth and longitude.

The ocean model computes sea surface temperature inside its domain. Outside its domain the observed annual mean sea surface temperature is specified. Where the boundary of the ocean is not a land surface, along 28°S and 50°N and in parts of the western tropical Pacific, it is possible to have an abrupt transition from calculated to specified sea surface temperatures. This is avoided by modifying the calculated sea surface temperatures within 1200 km of such artificial boundaries to ensure a smooth transition. The buffer zones near the southern and northern walls resolve this problem. In the case of the artificial western wall, shown in Fig. 1 for example, we interpolate linearly along a circle of latitude from the specified value at the wall to the calculated value 1200 km from the wall. Because the grid spacing in the ocean model is far denser than it is in the atmospheric model, the lower boundary condition for the atmospheric model is obtained by averaging sea surface temperatures spatially over areas corresponding to grid boxes of the atmospheric model. The coupling algorithm used in this experiment has been described in section 2 of Lau et al. (1992).

The initial conditions correspond to an atmosphere at rest. The tropical ocean has been initiated from a state of rest and the observed climatological density field. Once integrations with the coupled model start, the atmosphere provides heat flux across the ocean surface; but the salinity flux across the surface is specified to be zero. Inspection of the density field at different times during the integration indicated that salinity had a negligible effect on density gradients.

When integrations start, the motionless atmosphere does not have winds to maintain the density gradients and currents in the ocean. In particular, the eastward pressure force near the equator in the ocean, associated with the sloping thermocline, is unbalanced. As a consequence, the warm surface waters of the western equatorial Pacific immediately surge eastward so that the first El Niño develops because of an initial dynamical imbalance between the ocean and atmosphere.

The only external forcing is the annual mean solar radiation so that the model has no seasonal cycle. The coupled model was run for a total of 28 years. Because of problems with saving certain datasets during the first 7 years, only data from the last 21 years of the run could be analyzed in detail. The time-mean conditions described in the next section, for example, are for the last 21 years.

3. Time-averaged conditions

Figure 1a depicts the time average of the simulated sea surface temperature field in the tropical Pacific together with the temperatures that are specified for the rest of the oceans. The salient feature of the calculated field is the low temperatures in the southeastern tropical Pacific off the coasts of Peru and Ecuador. The cool surface waters extend across the equator, which is

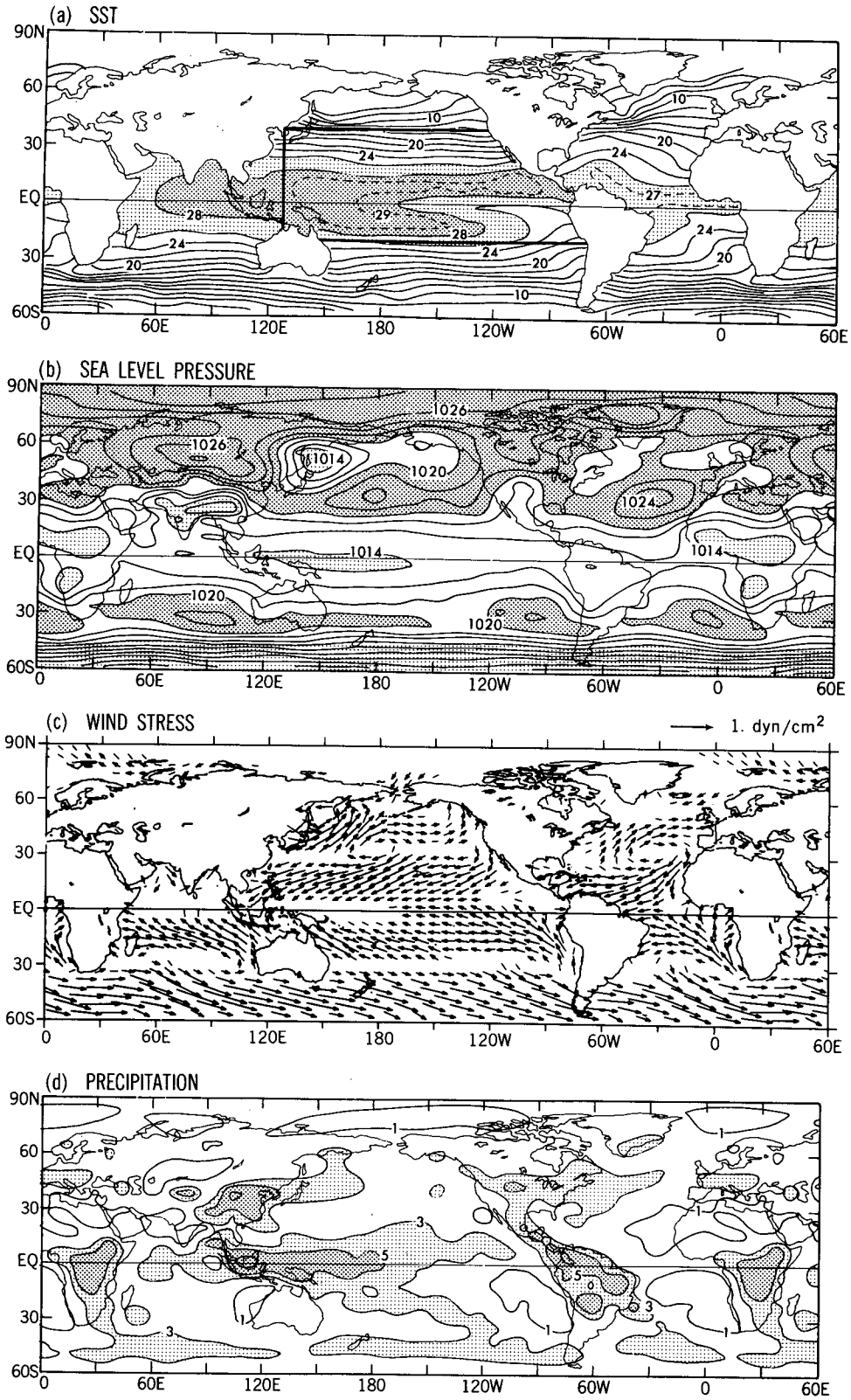

FIG. 1. Time-averaged values of (a) sea surface temperature (°C), which is specified except in the ocean model domain enclosed by the heavy, straight black lines in the tropical Pacific Ocean, (b) sea level pressure (contour interval 2 mb); (c) surface wind stress vectors with the scale given by the arrow in the upper right corner; and (d) rainfall, which is between 3 and 5 mm day^{-1} in lightly stippled areas and in excess of 5 mm day^{-1} where stippling is dense.

therefore south of the thermal equator—the line of maximum sea surface temperature. This sea surface temperature pattern affects the sea level pressure field shown in Fig. 1b because the subtropical high pressure zone is displaced equatorward in the southeastern Pacific (relative to its counterpart in the Northern Hemisphere). There is a corresponding asymmetry in the surface wind vectors in Fig. 1c: the southeast trade winds penetrate into the Northern Hemisphere and meet the northeast trades along an intertropical convergence zone (ITCZ) just north of the equator. In reality, the ITCZ is a zone of heavy precipitation, but in the model it is barely evident in the eastern tropical Pacific (Fig. 1d). In the Pacific the heavy rainfall is predominantly in the west, over the Indonesian Archipelago, where surface pressures are low. Arid conditions prevail in the regions of high surface pressure off the western coast of the Americas. All these climatological features are in reasonable agreement with observations, although simulated amplitudes are generally too small. For example, the surface wind stress over the tropical Pacific is weaker, by approximately 30%–40%, than those documented by Hellerman and Rosenstein (1983), and is also weaker than those described by Harrison (1989). Outside the tropical Pacific, where sea surface temperatures are specified, the simulated time-averaged meteorological fields are very similar to those in the simulation described by Lau (1985).

The sea surface temperature pattern in Fig. 1a is not merely a surface feature but reflects the subsurface thermal structure to some extent. In Fig. 2 is a map of the depth of the thermocline as measured by the oceanic temperature integrated vertically over the upper 317 m. Regions where the thermocline is shallow, the southeastern tropical Pacific and north of approximately 15°N, are also regions of low sea surface temperature. Where the thermocline is deep, in the western tropical Pacific, sea surface temperatures are generally high. The sea surface temperature gradient along the equator is associated with a thermocline that slopes downward to the west, as is evident in Fig. 3a. This slope implies an eastward pressure force that drives the eastward Equatorial Undercurrent in Fig. 3b. This current is an order of magnitude more intense than the one in the coarse-resolution model described by Lau et al. (1992), primarily because of the much lower dissipation in this high-resolution model. In comparison with measurements, however, the current is too weak by approximately a factor of 2. Not only the Equatorial Undercurrent but also the westward surface flow at the equator and the eastward North Equatorial Countercurrent immediately to the north are weaker in the model than in reality, presumably because the surface winds are too weak. A meridional section of the isotherms in Fig. 4a reflects the geostrophic balance of the zonal currents. For example, the upward slope of isotherms northward of approximately 3°N is associated with the eastward North Equatorial Countercurrent. The steep rise of shallow isotherms near the equator is indicative of both upwelling, which Fig. 4d confirms, and westward geostrophic flow. The equatorial trough of the deeper isotherms in Fig. 4a suggests that the Equatorial Undercurrent is in geostrophic balance. The poleward surface flow in both hemispheres in Fig. 4c corresponds to Ekman drift induced by the easterly winds. The equatorward subsurface flow is in geostrophic balance with the east–west slope of the isotherms. The currents and thermal structure in Fig. 4 are reasonably realistic, except for the absence of a ridge in the isotherms near 10°N. [See Philander (1990) for similar figures based on measurements.] In reality, isotherms deepen to the north of 10°N, a region in which the geostrophic surface flow is westward. This motion is the southern branch of the subtropical oceanic gyre that includes the Kuroshio Current. The model resolves this southern branch poorly, in part because of the coarse resolution north of 10°N and because the associated high lateral mixing diffuse the conditions imposed along the artificial northern boundary equatorward. The wind-stress curl accompanying the diffuse ITCZ may also contribute to this deficiency.

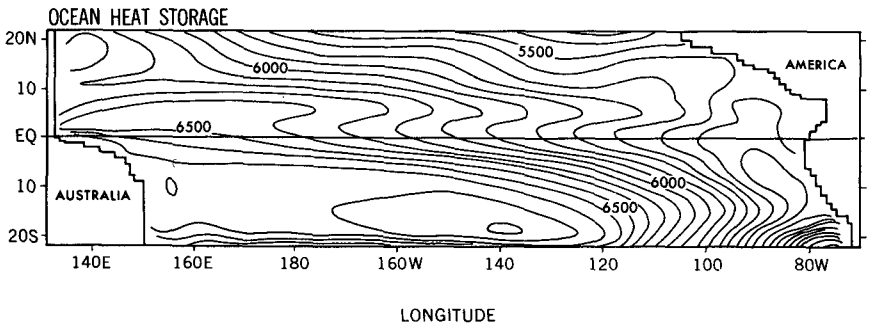

FIG. 2. Time-averaged heat storage (°C m) as measured by the vertical integral of the oceanic temperature to a depth of 300 m.

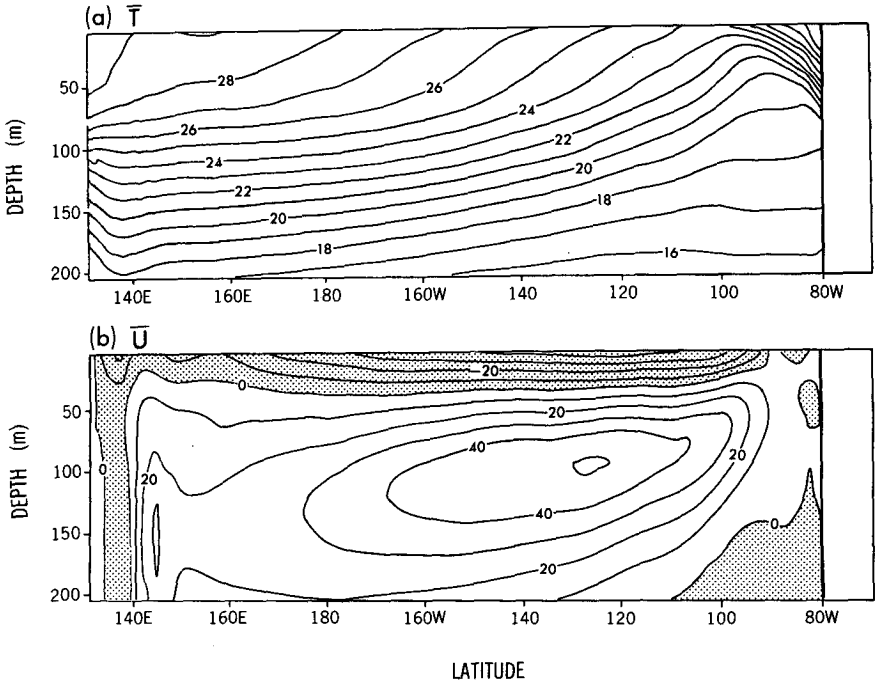

FIG. 3. Time-averaged values of (a) temperature (°C) and (b) zonal currents (10^{-2} cm s^{-1}) in the equatorial plane. Motion is westward in shaded areas.

4. The simulated Southern Oscillation

Although the external forcing for the coupled model is steady, its response has variability over a broad spectrum of frequencies. Some of this variability appears in Fig. 5. A fluctuation with a time scale on the order of 5 years is the most prominent low-frequency signal in the time series shown in Fig. 5. The simulated atmospheric and oceanic phenomena on such interannual time scales will be described in detail in the present section, and the discussion of the higher-frequency features will be deferred until section 5.

It is evident in Fig. 5 that, on long time scales, different parameters vary practically in phase so that periods of high sea surface temperature in the tropical Pacific coincide with a thermocline that is locally deep. (We shall later see that the compensating elevation of the thermocline occurs off the equator in the western tropical Pacific.) At such times the trade winds are relaxed, there is heavy precipitation over the central equatorial Pacific, and sea level pressure difference between Darwin (Australia) and Tahiti is small. During periods of low sea surface temperature in the eastern tropical Pacific, tendencies are in the opposite direction. Similar correlations between various atmospheric and oceanic parameters characterize the observed Southern Oscillation (Rasmusson and Carpenter 1982). It is of special significance that changes in sea surface temperature, the only oceanic parameter that affects the atmosphere, and changes in the surface winds, the principal forcing function for the ocean, are practically in phase, as is evident in Fig. 6. An eastward surge of warm surface waters coincides with the eastward penetration of westerly winds or a weakening of the trades, especially in years 12 and 13, while westward penetration of low sea surface temperatures coincides with intense easterly winds. The interannual fluctuations clearly are not a property of one medium, with the other responding passively, but must involve interactions between the ocean and atmosphere.

The coupled model realistically reproduces not only the temporal but also the spatial structure of the Southern Oscillation. (Even though this model has no seasonal cycle, 1 year = 12 months was chosen as a unit of time and the usual names for the months are retained.) In Figs. 7–11, the contrast between conditions at the peak of a warm El Niño phase (March of year 13 of the simulation, for example) and conditions at the peak of a cold La Niña phase (June of year 15, for example) illustrates the spatial structures. Although these two episodes have the largest amplitude in the simulation, their structures are representative of the structures of weaker episodes. In Figs. 7a and 7b, large sea surface temperature changes occur principally in the eastern tropical Pacific where a tongue of cold surface waters is well developed during La Niña and is practically absent during El Niño. (The waves, evident on the 26°C isotherm in the region north of the equator, are associated with an instability attributable to the large latitudinal shear of the westward surface cur-

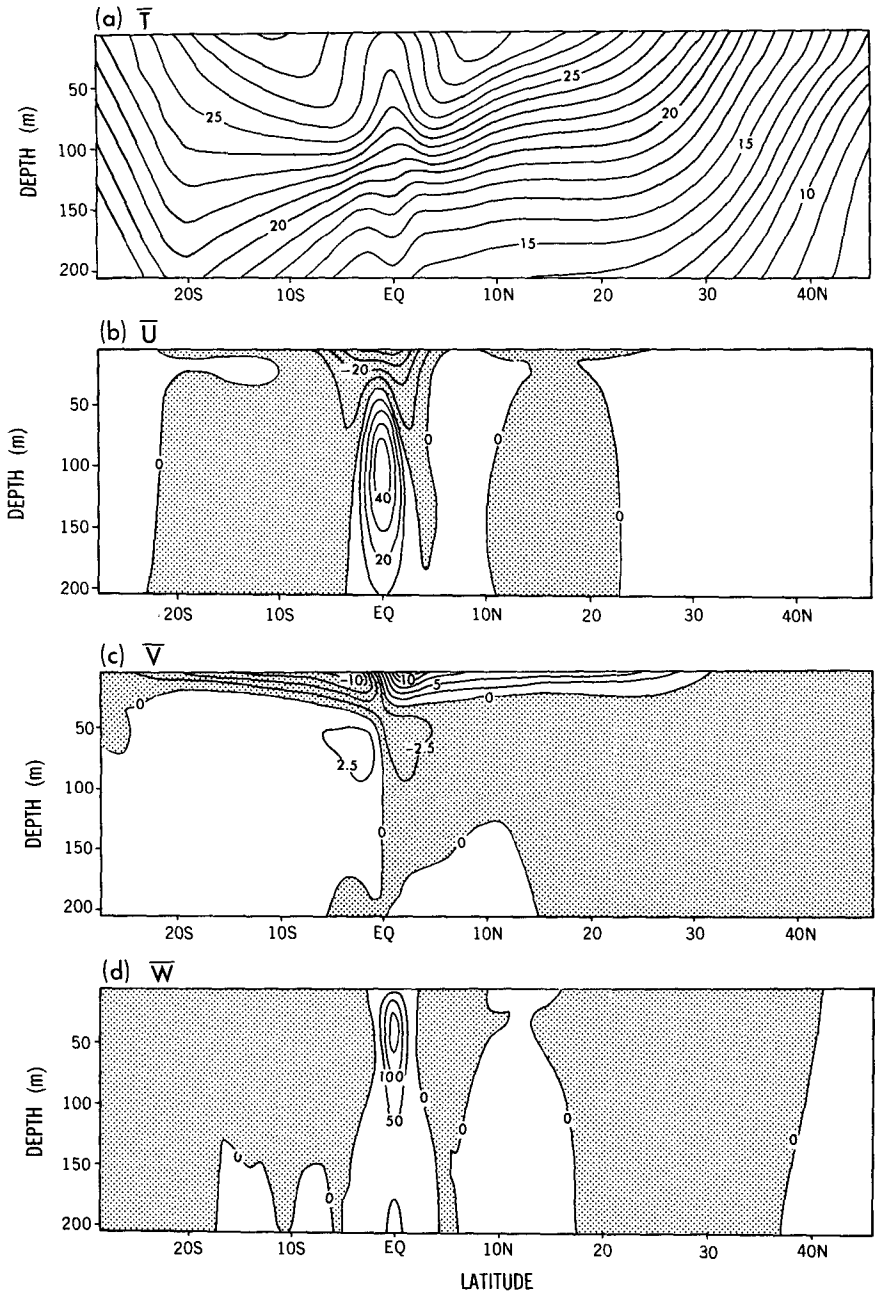

FIG. 4. Time-averaged values of the oceanic (a) temperature (°C), (b) zonal current (10^{-2}cm s^{-1}), (c) meridional current (10^{-2} cm s^{-1}), and (d) vertical velocity component (10^{-2} cm day^{-1}) in the plane of 135°W in the central Pacific. Motion is westward, southward, or downward in shaded areas.

rent at the equator.) The change in sea surface temperature is not merely a surface phenomenon but involves a substantial east–west redistribution of warm upper-ocean waters. It can be seen in Figs. 8a and 8b that thermocline depth variations in the eastern and western tropical Pacific are out of phase. Unlike sea surface temperature changes, which are small in the west, those in thermocline depth are large both in the west and in the east. The changes in the currents that accompany this interannual horizontal redistribution of warm surface waters are depicted in Fig. 9. The westward transport of the surface flow near the equator is large during La Niña when the thermocline is deep in the west and shallow in the east and is more modest during El Niño when anomalous eastward surface currents, which return some of the warm surface waters

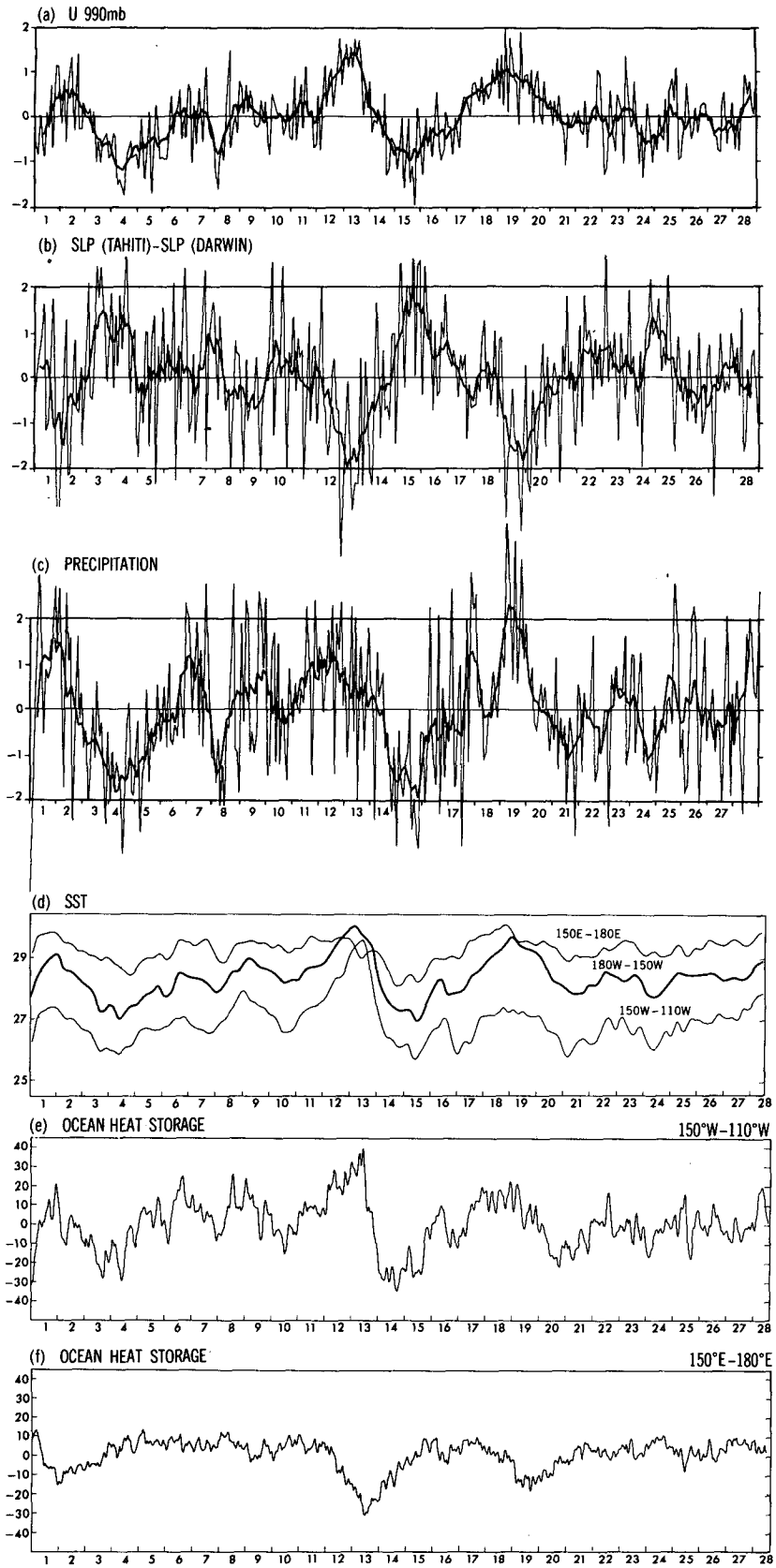
(a) U 990mb
(b) SLP (TAHITI)-SLP (DARWIN)
(c) PRECIPITATION
(d) SST
150E-180E
180W-150W
150W-110W
(e) OCEAN HEAT STORAGE
150°W-110°W
(f) OCEAN HEAT STORAGE
150°E-180°E

in the west to the east, are more prevalent. The change in the zonal slope of the thermocline between El Niño and La Niña affects the intensity of the Equatorial Undercurrent that is driven by zonal pressure gradients. In Fig. 9 this current is weak during El Niño when the pressure force is weak and is intense during La Niña when the force is large. Figure 9 also shows the changes in the meridional structure of the thermal field. The salient feature, the pronounced shoaling of shallow isotherms near the equator during La Niña, is indicative of enhanced upwelling at that time.

The meteorological changes associated with the simulated Southern Oscillation are in accord with observations and can be explained as the response of the atmosphere to the sea surface temperature changes. During La Niña, when the warmest surface waters along the equator are confined to the west, moist air converges into that region, which has low sea level pressure and heavy precipitation, as is evident in Figs. 10 and 11. The trade winds are intense at such times when sea level pressure is high in the southeastern tropical Pacific. During El Niño, when most of the tropical Pacific Ocean is covered with warm surface waters, the pressure gradient across the equatorial Pacific decreases, primarily because sea level pressures over the southeastern tropical Pacific fall. The region of heavy precipitation now moves eastward, and the trade winds relax. There is a hint from observations of northerly wind anomalies at some longitudes along the equator during El Niño. This is suggestive of a southward displacement of the ITCZ, but the grid size of the atmospheric model is too crude to resolve this feature.

In this model, the interannual variability in the tropical Pacific is associated with minor changes in the surface winds over the tropical Atlantic and Indian oceans. The occurrence of El Niño in the Pacific is accompanied by a decrease in rainfall over the Amazon basin, over Indonesia, and over parts of central and southeastern Africa. Some of these results are evident in Fig. 11c.

The Southern Oscillation, in this simulation, is characterized by large sea surface temperature changes in the central and eastern equatorial Pacific. In Fig. 12 there is no consistent zonal phase propagation in either sea surface temperature anomalies or zonal wind anomalies. Eastward phase propagation is pronounced in the thermocline depth variations along the equator (as indirectly inferred from Fig. 13a), but it is confined to the western side of the basin where the speed is approximately 15 cm s^{-1}. Off the equator, along 10°N for example, phase propagation is absent in the west but is present and is westward near the coast of Central America (see Fig. 13b). The speed is approximately 6 cm s^{-1}. The structure of thermocline displacements is interestingly different in the western and eastern tropical Pacific. Although thermocline displacements are symmetrical about the equator both in the east and west, they have an equatorial maximum in the east but an equatorial minimum and off-equatorial maxima near 8°N and 8°S in the west, as is evident in Figs. 8 and 14. To explain these features, it is necessary to inspect the surface winds.

In Fig. 12, changes in the zonal wind stress along the equator have their maximum amplitude west of the maximum sea surface temperature anomalies. The response of this particular atmospheric model to anomalously warm surface waters in the central and eastern equatorial Pacific includes a relatively narrow jet of westerly winds to the west of the warm water. In Fig. 11c, which contrasts the zonal winds at the peaks of a warm El Niño and cold La Niña, the latitudinal shear of the wind anomaly is seen to be very large. During warm episodes, the westerly winds near the equator cause a divergence of the surface waters near 8°N and 8°S so that the thermocline shoals near those latitudes. The same winds drive equatorward Ekman drift, and this water is then transferred eastward by equatorial currents. As a result, thermocline variations shown in Figs. 8 and 14 are symmetrical about the equator, with maxima near 8°N and 8°S in the west. In the east, on the other hand, thermocline displacements are a consequence not primarily of the local wind forcing but of eastward advection along the equator. The thermocline displacements are therefore maximized about the equator in the east.

The time–space evolution of the sea surface temperature and surface wind anomalies are rather complicated and do not provide strong clues concerning the switch from warm to cold conditions and back again to warm conditions. Variations in thermocline depth are far more consistent and interesting because

FIG. 5. Time series of the following variables: (a) the zonal wind anomalies (m s^{-1}) at 990 mb averaged over the equatorial zone (4.5°S to 4.5°N) of the central Pacific Ocean (165°E to 165°W); (b) the Southern Oscillation pressure index (in mb) defined as the difference between the surface pressures at the grid points corresponding to Tahiti and Darwin; (c) precipitation anomalies (mm day^{-1}) averaged over the equatorial zone (4.5°S to 4.5°N) of the central Pacific Ocean (165°E to 165°W); (d) sea surface temperatures in the warm western and colder eastern equatorial Pacific. The curves are 7-month running means of areal averages for the equatorial zones (4.5°S to 4.5°N) bounded by 150°E and 180° (top), 180° and 150°W (middle), and 150°W and 110°W (bottom). (e) Heat storage anomalies (the volume integral of temperature to a depth of 315 m) in the eastern equatorial Pacific, the zone 2.5°S to 2.5°N and 150°W to 110°W in units of 10^{20} joules; (f) heat storage anomalies in the eastern equatorial Pacific, the zone 2.5°S to 2.5°N and 150°E to 180°E. The thin curves in (a), (b), and (c) are monthly mean values, the heavy lines are 13-month running means of the monthly data. The curves in (e) and (f) are low-pass filtered to eliminate fluctuations with periods less than 2 months.

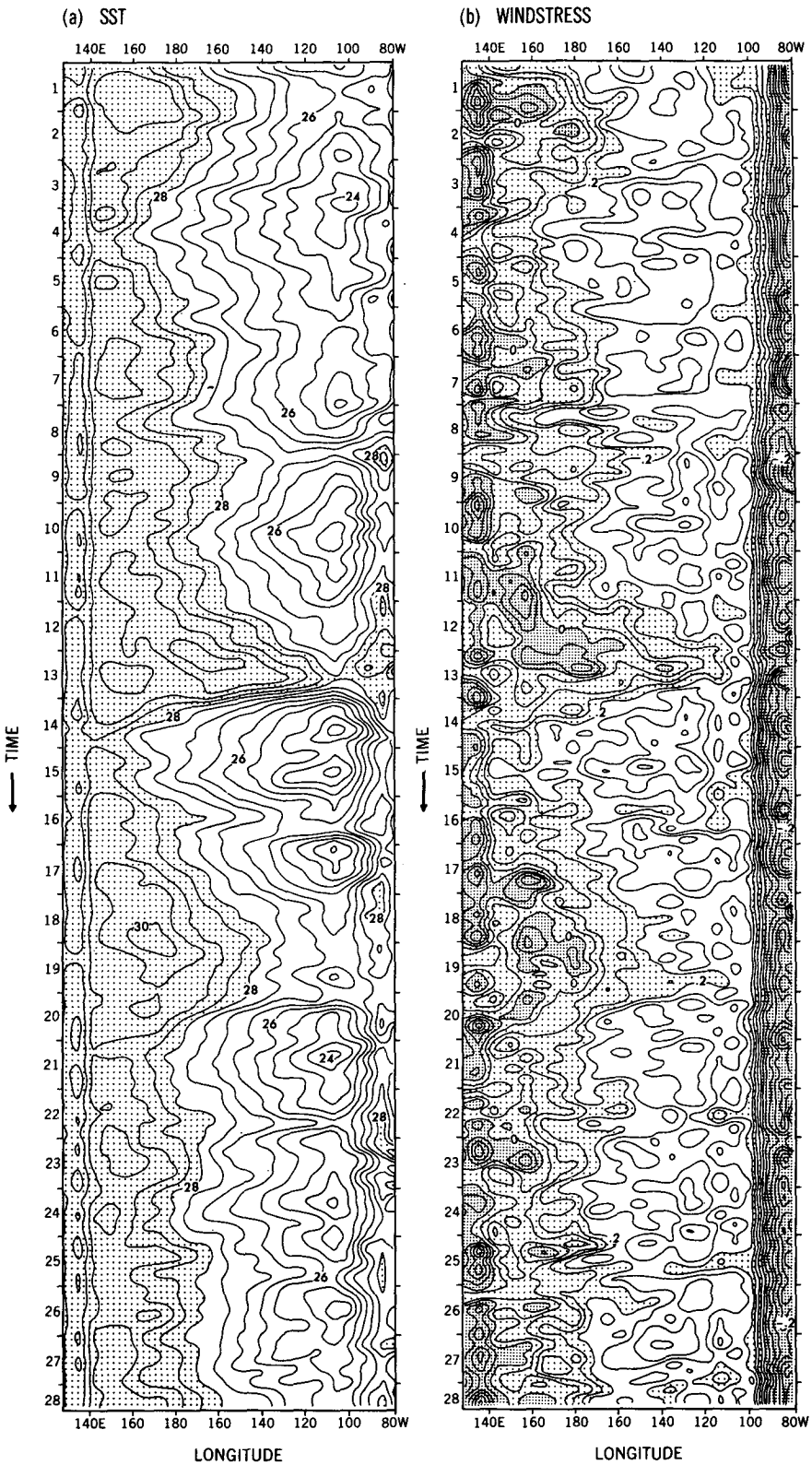

FIG. 6. Variations (13-month running means) in sea surface temperature (°C) and zonal wind stress (dyn cm^{-2}) along the equator. In shaded regions temperatures exceed 28°C and the easterly winds are weaker than 0.2 dyn cm^{-2}. The winds are westerly in shaded areas.

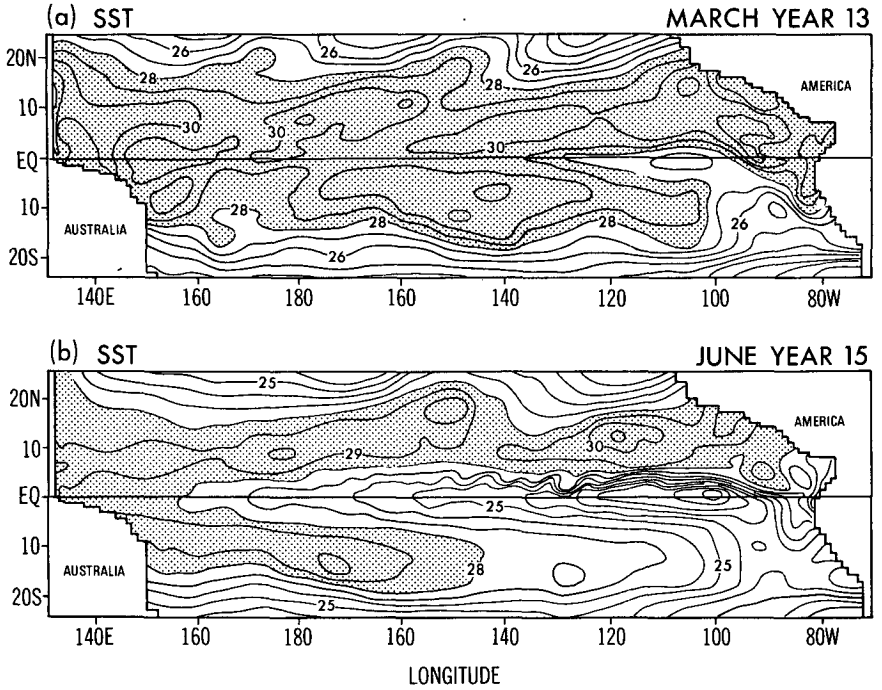

FIG. 7. Sea surface temperature (°C) at the peak of a warm El Niño episode in March of year 13 (a) and at the peak of a cold La Niña episode in June of year 15 (b). Note that even though the model examined here has no seasonal cycle, 1 year = 12 months was chosen as units of time, and the usual names for the months in this and some of the following figures have been retained.

they have eastward phase propagation in some regions—the western equatorial Pacific—and westward phase propagation in others—the off-equatorial eastern Pacific, for example. The phase speeds, 15 and 6 cm s^{-1} in Figs. 13a and 13b, respectively, are too slow to be identified with a single equatorial Kelvin or off-equa-

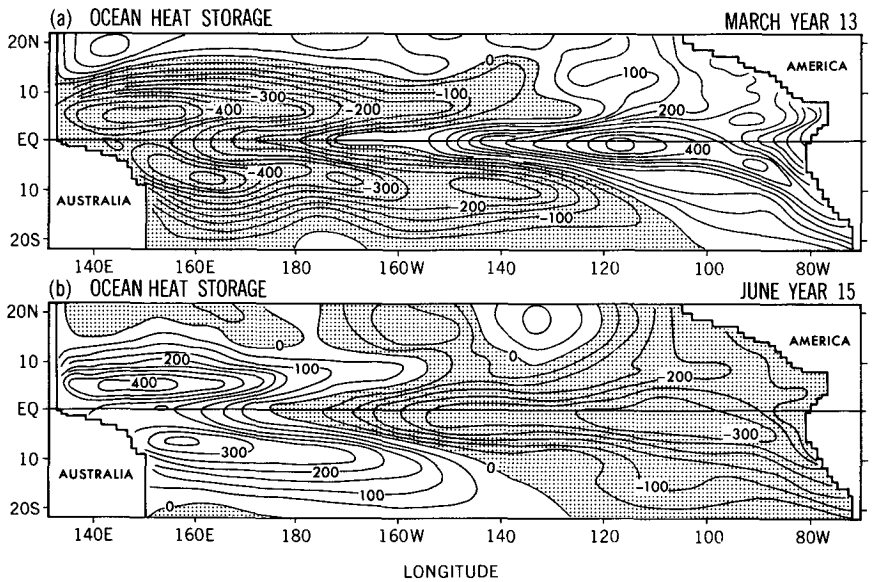

FIG. 8. As in Fig. 7, but for heat storage anomalies (°C m) relative to the time-averaged field of Fig. 2. The thermocline is elevated in shaded regions.

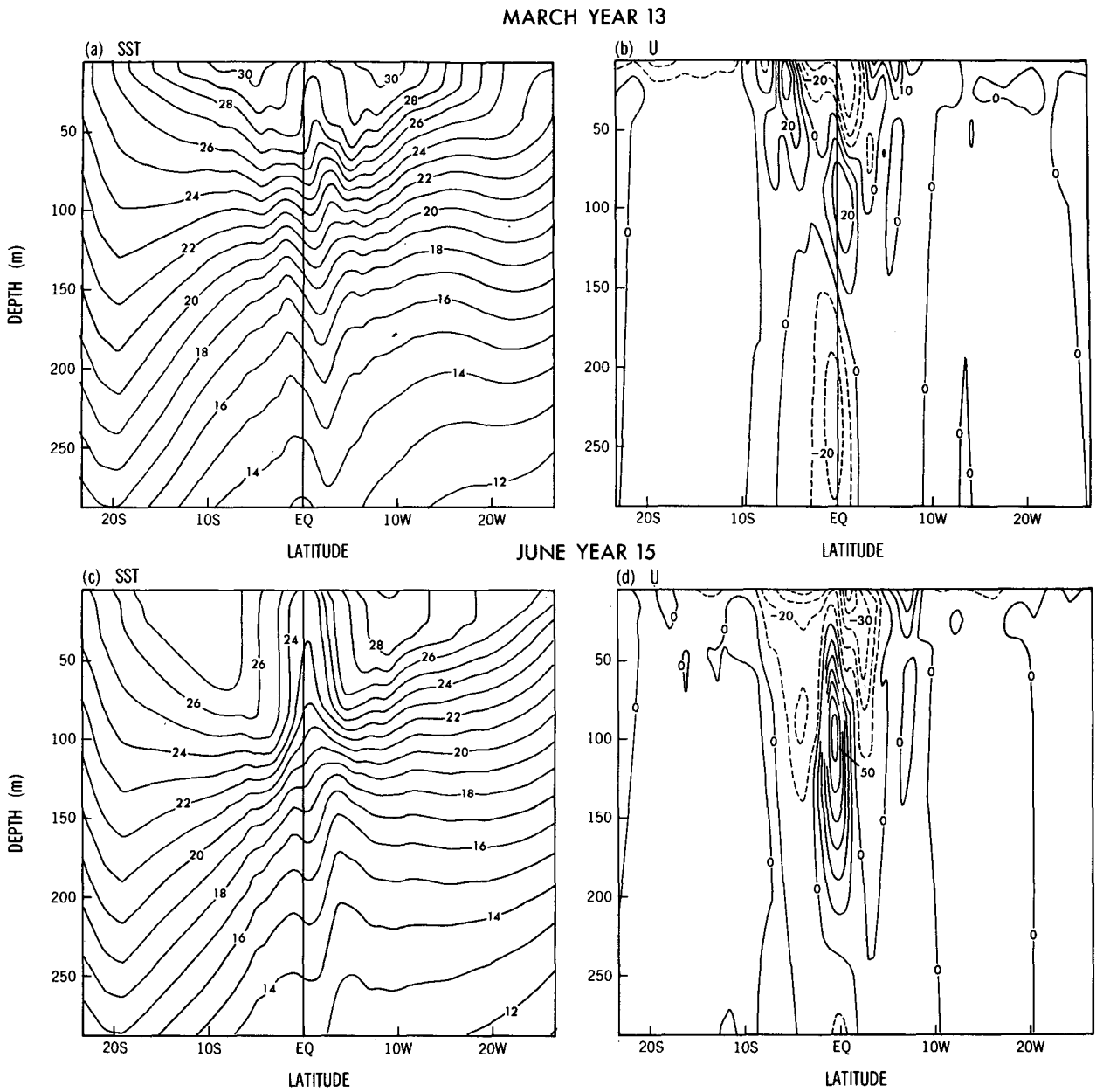

FIG. 9. The temperature (°C) and zonal currents (10^{-2}m s^{-1}) in the central Pacific along 136°W at the peak of an El Niño episode in March of year 13 in (a) and (b) and at the peak of a La Niña episode in June of year 15 in (c) and (d). Dashed contours indicate westward flow.

torial Rossby wave. To explain these phase speeds it is necessary to keep in mind that the ocean is being forced by quasi-periodic winds. These winds directly drive currents and excite a host of waves. If the period of the forcing were on the order of a few weeks, then only equatorial Kelvin waves would be available for excitation (Philander and Pacanowski 1981). With increasing period more and more Rossby waves come into play: the pattern of phase propagation can become very complex, and it is no longer possible to identify an individual (Kelvin or Rossby) wave. This is the case in Fig. 13. If the period of the forcing becomes very long, then the picture simplifies because the ocean is in equilibrium with the winds and, at each moment, is essentially in a steady state. Evidence of phase propagation (and hence of waves) then disappears. The waves are, of course, implicitly present because they have brought the ocean into a state of adjustment with the wind on a time scale very short in comparison with the time scale of the wind fluctuations. In such a case the oceanic response is an equilibrium one and at any given time has no "memory" of the winds at earlier

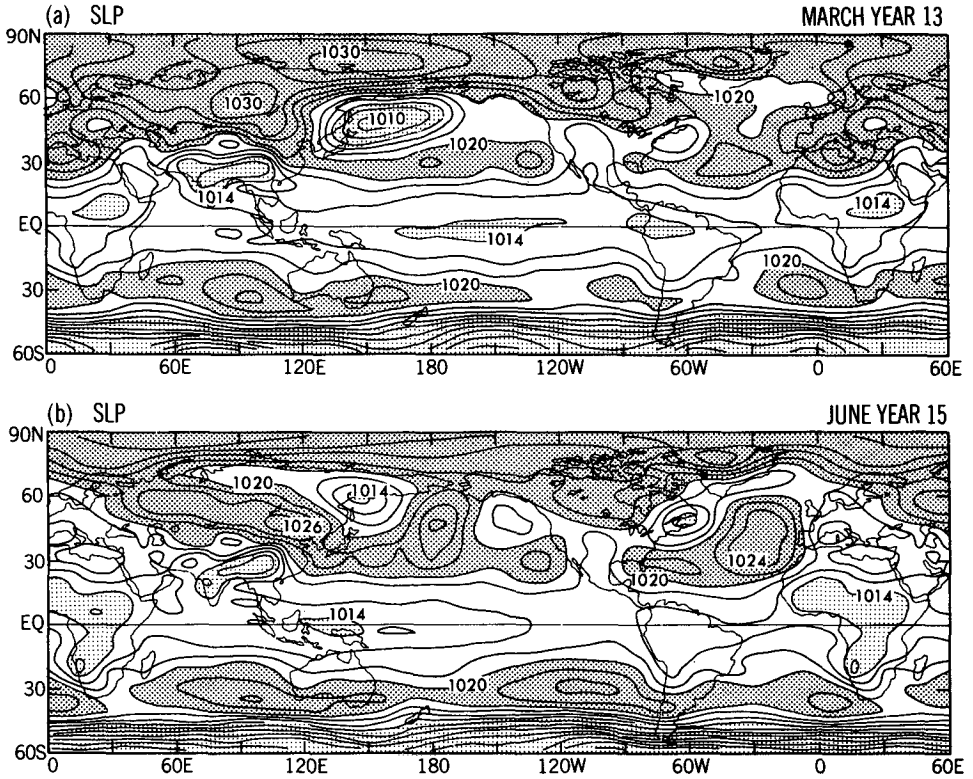

FIG. 10. Changes in sea level pressure patterns (contour interval: 2 mb) between El Niño conditions of March of year 13 (top) and La Niña conditions of June of year 15.

times. If, at a certain time, the winds were held fixed, then the ocean would experience no further adjustment and would remain in a steady state. The phase propagation evident in Fig. 13 indicates that in the case of the simulated Southern Oscillation, the oceanic response to the slowly varying surface winds is not an equilibrium one. If at a certain time, in year 13 during El Niño, say, the winds were held fixed, then the ocean would continue to adjust. We can anticipate that the elevation of the thermocline in the west in year 13 in Fig. 13a would continue its eastward propagation. In due course this would elevate the thermocline in the east and affect sea surface temperatures. If ocean–atmosphere interactions are permitted, then this could lead to the termination of El Niño and the onset of La Niña.

5. The quasi-resonant oceanic mode

Energetic vertical movements of the thermocline, with a period near 7 months, are clearly evident in Fig. 5e. (An energy spectrum of this record has a pronounced peak at a period of 7 months.) Unlike the low-frequency oscillations of section 4, these fluctuations are not characterized by a significant correlation between surface wind and sea surface temperature variations, and there is no persuasive evidence that they are attributable to ocean–atmosphere interactions. The 7-month oscillations are primarily an oceanic phenomenon. The wind fluctuations on that time scale do not appear to be well organized, although it is possible that more sophisticated analyses will indicate that the wind variations are not entirely random and have a component with a coherent structure. In this paper our attention is confined to an exploration of the hypothesis that the 7-month oceanic oscillation is a quasi-resonant mode of the ocean, excited by intermittent wind fluctuations.

Inspection of a sequence of maps of the vertically averaged temperature, of the type in Fig. 15, reveals that these oscillations are associated with depressions of the thermocline that travel eastward along the equator. This figure depicts the history of a particularly energetic pulse, that in August of year 8. As early as December of year 7 two westward-traveling depressions of the thermocline are evident just off the equator in the western Pacific. By April of year 8 they have formed a deep pool of warm surface waters at the western boundary near the equator. The eastward-traveling pulse of August then transfers much of the water in this pool to the eastern side of the basin, where it starts to disperse poleward along the coast and also westward back into the oceanic interior. If the westward-traveling disturbances were to reach the western boundary and

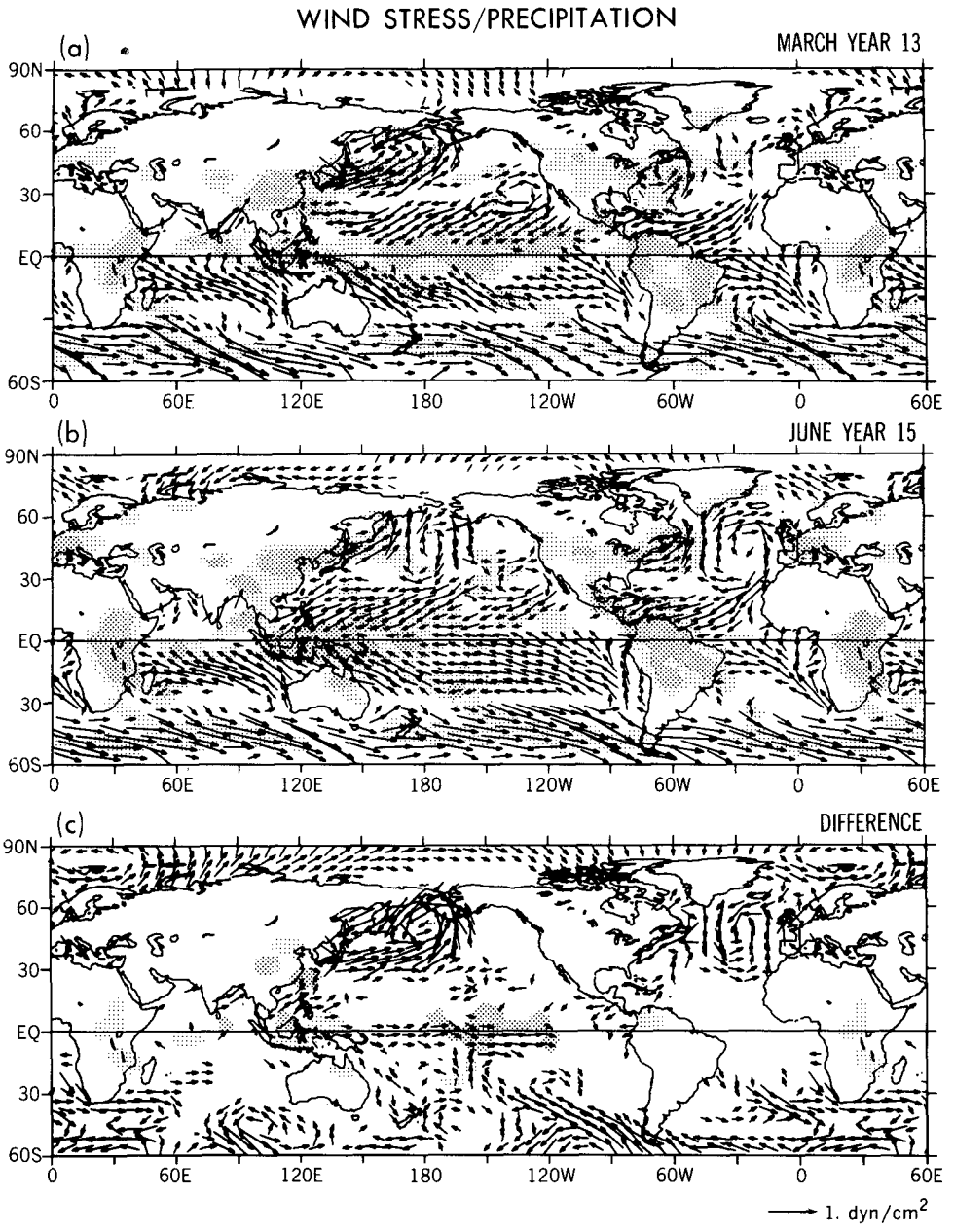

FIG. 11. The surface windstress during El Niño of March of year 13 (top) and during La Niña of June of year 15 (middle). The bottom figure shows the difference between these conditions. Arrows too short to show up clearly have been omitted. In panels (a) and (b), light stippling indicates precipitations between 3 and 5 mm day^{-1}, and dense stippling indicates values exceeding 5 mm day^{-1} In panel (c), light and dense stippling indicate precipitation differences of -3 and $+3$ mm day^{-1}, respectively.

transform into an eastward equatorial pulse, then the period of the oscillation would be much longer than 7 months. This matter will be discussed later.

The structure of the oscillations just described is similar to that of the quasi-resonant oceanic mode discussed by Cane and Moore (1981). That mode is composed of an eastward-traveling equatorial Kelvin wave that reflects off the eastern boundary of the ocean basin as an equatorially trapped Rossby wave, which in turn reflects off the western boundary as an equatorial Kelvin wave. The period of the mode is the travel time of the waves. The gravity wave speed is c for the Kelvin wave and c/3 for the Rossby waves, so that the period is $4L/c$ where L is the width of the basin. The mode is only quasi resonant (not perfectly resonant) because reflections at the eastern boundary are associated with a poleward loss of energy; an incident Kelvin wave excites poleward-traveling coastally trapped waves in

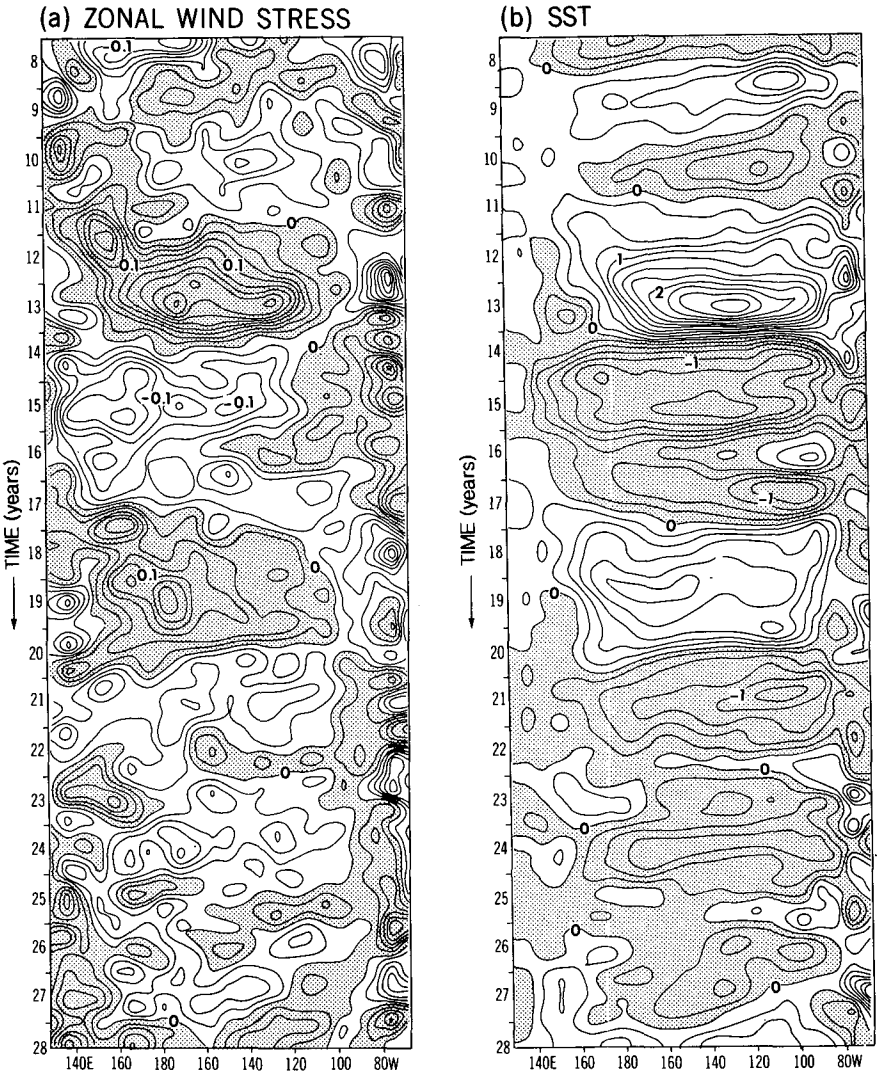

FIG. 12. Sea surface temperature (°C) and zonal wind stress (dyn cm^{-2}) anomalies along the equator. Shading indicates westerly wind stress and negative temperature anomalies. The data have been low-pass filtered to isolate fluctuations with periods longer than 2 years.

addition to the reflected equatorially trapped Rossby waves. These modes are readily excited when a shallow-water model is forced with winds that abruptly start to blow and then remain steady. [See, for example, Fig. 3.19 of Philander (1990).]

In the case of the coupled model under discussion here, the eastward-traveling pulses along the equator have the vertical structure of the second baroclinic mode and travel with a speed of approximately 150 cm s^{-1}. The period of the quasi-resonant mode should therefore be on the order of 15 months. In Fig. 5e, however, the oscillations have a period near 7 months. This discrepancy would be explained if there were two of the quasi-resonant modes present simultaneously with the Kelvin wave of the one propagating eastward along the equator, while the Rossby waves of the other were traveling westward. Figure 16 suggests that this is indeed happening but that the oscillations are far more irregular than in the idealized case. In July and August of year 8 there is an eastward-traveling depression of the thermocline and, in due course, this depression reappears as a westward-traveling disturbance that is more prominent near 6°N and 6°S than near the equator. After reaching the western coast around September of year 9, it is associated with the appearance of another Kelvin wave in the west. Before that happens, however, another equatorial depression of the thermocline appears in December of year 8 and January of year 9. In other words, two quasi-resonant oceanic modes are present simultaneously, so that the model data on the equator reveal oscillations with a period of 7, rather than 14, months. Further analyses

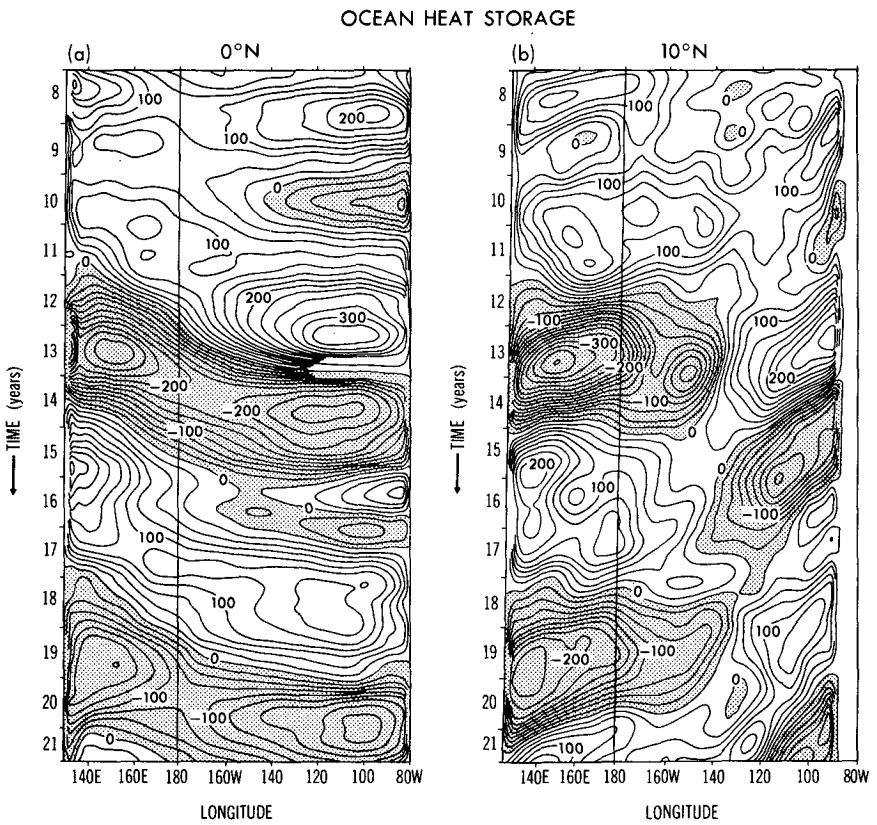

FIG. 13. Variations in heat storage (°C m) anomalies (as measured by the temperature integrated vertically to a depth of 300 m, along the equator and along 10°N. The data have been low-pass filtered to isolate fluctuations with periods longer than 2 years. The thermocline is elevated in shaded areas.

of the data are necessary to determine why two, rather than three or four, of these modes are present simultaneously. It is possible that nonlinear interactions play a role.

The modes under discussion are quasi resonant because every reflection at the eastern wall of the ocean basin is accompanied by a poleward loss of energy. It is therefore necessary to inquire into the maintenance of the mode. Figure 17 indicates that high-frequency wind fluctuations near the equator play a crucial role. The pattern in Fig. 17a indicates that bursts of westerly winds along the equator have irregularities in the time and place of their occurrence. In Fig. 17b, some of the bursts are seen to generate intense eastward equatorial jets with which the depressions of the thermocline in Fig. 16a are associated. The wind burst of June of year 8 amplifies the quasi-resonant oceanic mode, as does the wind burst of January of year 9. But the bursts of August of year 8 in the far west do not seem to influence the quasi-resonant modes. However, the burst of a few weeks later, October of year 8, in the east clearly affects the timing of reflections at the eastern coast. Instead of starting there in September of year 8, it is delayed until after the wind burst of October. The conclusion is that the modes are sustained and are also made irregular by high-frequency wind fluctuations. The fluctuations last a few weeks—less than the approximately 3 months it takes a Kelvin wave to propagate across the ocean—and have a spatial scale on the order of 1000 km. These wind fluctuations that sustain the quasi-resonant oscillations were apparently filtered from the monthly mean winds that forced an identical ocean model in a simulation of the seasonal cycle (Philander et al. 1987). The quasi-resonant modes are absent from that model.

In principle, reflections off the western wall of the ocean basin are an essential part of a resonant mode. In the simulations, however, there are occasions when a burst of westerly winds can eliminate these reflections by inducing equatorward Ekman drift so that a depression of the thermocline is transferred to the equator from off-equatorial latitudes without involving the coast at all.

The quasi-resonant oceanic modes do not involve interactions between the ocean and atmosphere but form part of the passive response of the ocean to forcing. Sometimes this response has a sea surface temperature signature. The modest warmings of the eastern

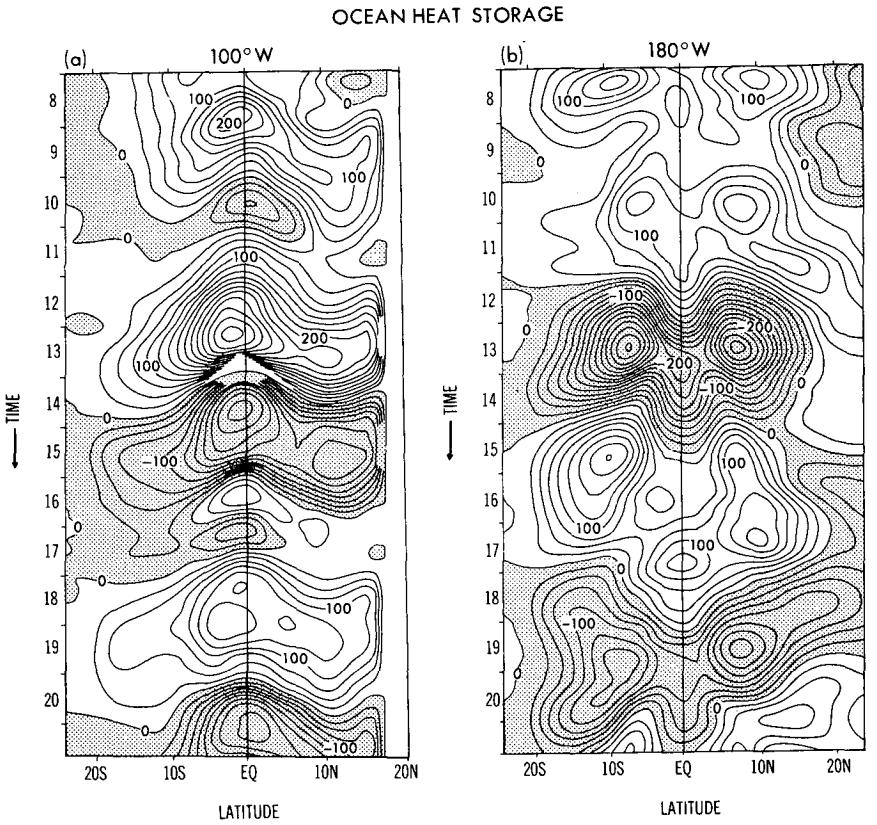

FIG. 14. As in Fig. 13, but along 100°W in the eastern and 180° in the western tropical Pacific.

tropical Pacific at the end of year 8 and again in year 16, evident in Fig. 5d, are associated with the quasi-resonant oceanic modes and are distinct from the interannual warm El Niño episodes, attributable to interactions between the ocean and atmosphere discussed in the previous section. Although they are distinct, the low-frequency oscillations and the quasi-resonant modes affect each other. For example, the abrupt termination of the intense El Niño episode, in year 13 in Fig. 5d, is to a large extent attributable to an equatorial Kelvin wave associated with the quasi-resonant mode that elevated the thermocline at the time.

Whether the quasi-resonant oceanic mode has a counterpart in reality is unclear. It could, on one hand, be an artifact of the highly idealized geometry of the model ocean basin, which has perfectly reflecting coasts. On the other hand, the period of 14 months is sufficiently close to that of the annual cycle for such a mode to be part of the observed annual cycle.

6. Discussion

The Southern Oscillation simulated in both the coupled model described in this paper (subsequently referred to as HR for high resolution) and the one with the global, low-resolution (LR) ocean described in Lau et al. (1992) are realistic in many respects. Not only the time-averaged states but also the variability, especially the interannual fluctuations in the tropics, resemble that which is observed. Despite these similarities the models simulate El Niño episodes that evolve in very different ways. In the LR model modest signals first appear in the eastern tropical Pacific off the coast of Peru and Ecuador, whereafter they migrate westward as they amplify. In due course anomalies of the opposite sign appear in the east and in turn migrate westward. In the HR model there is no consistent phase propagation in the zonal wind stress and sea surface temperature variations, but thermocline depth changes have phase propagation: along the equator it is eastward in the western Pacific; off the equator it is westward in the eastern Pacific. This simulated Southern Oscillation in HR corresponds to a coupled ocean–atmosphere mode, but it clearly is a mode different from the one excited in the LR coupled model. Why are different modes excited in the two models? What determines the period of the Southern Oscillation in the models? Why are the low-frequency oscillations irregular?

As stated in Lau et al. (1992), studies of the interactions between the ocean and atmosphere follow two complementary routes. One route is concerned with stability analyses that determine the spectrum of pos-

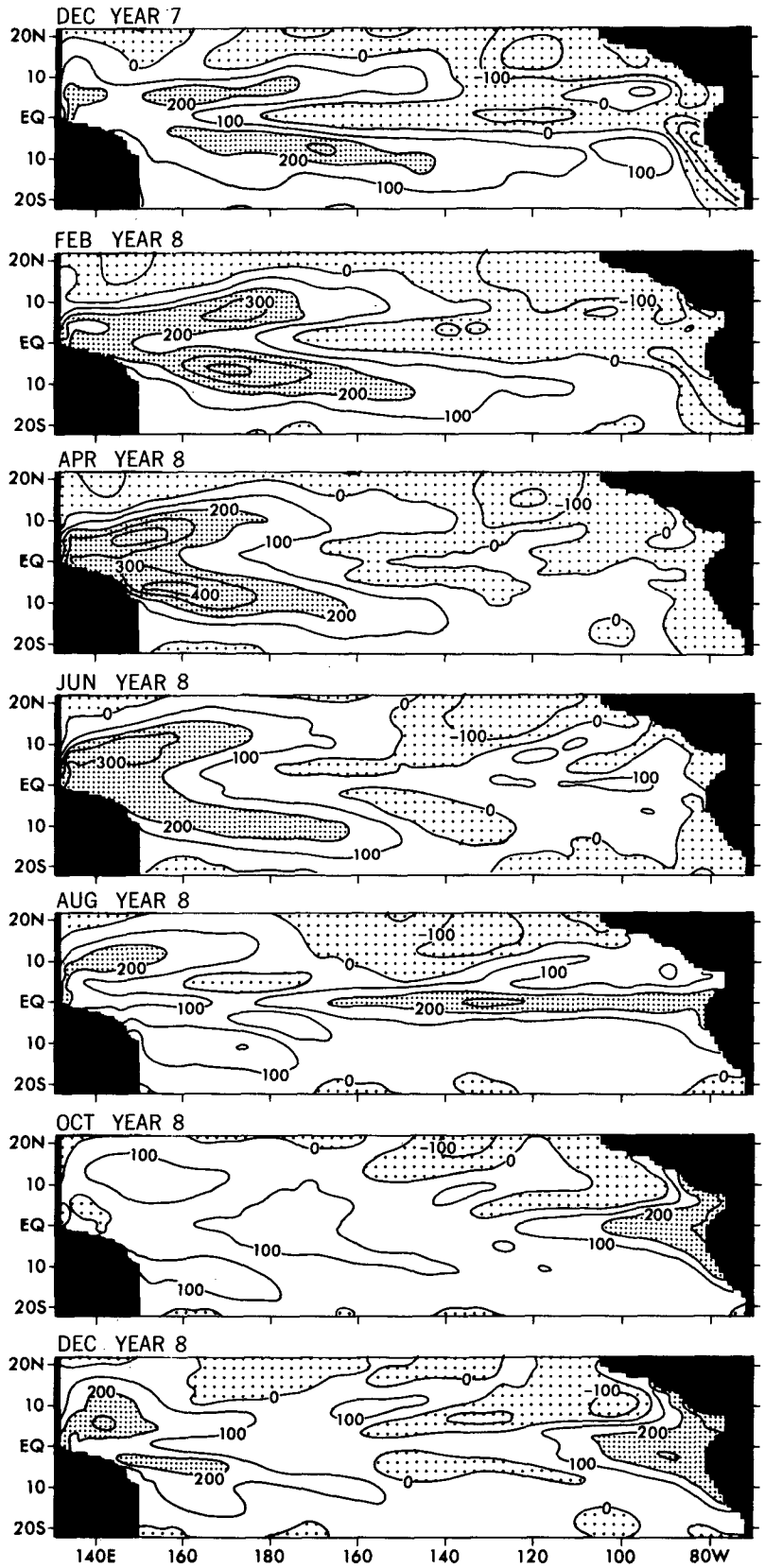
DEC YEAR 7
FEB YEAR 8
APR YEAR 8
JUN YEAR 8
AUG YEAR 8
OCT YEAR 8
DEC YEAR 8
20N
10
EQ
10
20S
140E
160
180
160
140
120
100
80W

sible unstable modes and their dispersion relations. The other route, the one followed in this paper, studies the excitation of one or more modes in coupled models that march forward in time. The dominant mode in one of these coupled models is presumably the mode that, according to stability analyses, has the largest growth rate. In idealized situations such a mode appears in isolation and is perfectly regular with a period that corresponds to that of the most unstable mode. Schopf and Suarez (1988) and Battisti (1988) realized such a state of affairs in their coupled models by suppressing "random" atmospheric fluctuations (such as weather) that are unrelated to ocean–atmosphere interactions. The simulated Southern Oscillation can be made irregular by introducing "weather." These results suggest that in the calculations described in this paper, the high-frequency fluctuations, including the quasi-resonant oceanic mode with a period near 7 months, contribute to the irregularity of the low-frequency Southern Oscillation.

Stability analyses of the interactions between the ocean and atmosphere indicate that there are at least two types of coupled modes. In the first class of modes, sea surface temperature and surface wind variations can be in phase but other oceanic parameters, thermocline depth variations, for example, have a phase lag that represents the inertia of the ocean or its "memory" of earlier winds to which it is still adjusting. Coasts, and hence the dimension of the ocean basin, are important because they affect oceanic adjustment. The HR model captures this type of mode, explained earlier, as do the models of Schopf and Suarez (1988), Cane and Zebiak (1985), and Battisti (1988). Schopf and Suarez (1988) and Battisti and Hirst (1989) propose, as an analog for the Southern Oscillation, the delayed oscillator equation

$$F_t = aF(t) - bF(t - \tau) - cF^3(t),$$

where the first term on the rhs represent local, unstable ocean–atmosphere interactions, and the next term represents the delayed response of the ocean because of its memory. This equation has amplifying, oscillatory solutions whose period depends on the delay time τ, which is sometimes interpreted to be literally the time it takes equatorial Rossby and Kelvin waves to propagate from the region of ocean–atmosphere interaction to the western coast and back. As mentioned earlier, explicit evidence of such isolated waves is plentiful in the HR model at relatively high frequencies but is absent if data are low-pass filtered to isolate the Southern Oscillation. Explicit evidence of waves is also absent from the simpler coupled models just mentioned. (It is of course possible to project any function that represents the response of the ocean, for example, onto the complete set of Hermite functions, which also happen to represent equatorial waves, but there is no evidence that the response of the ocean involves those waves.) The phase speeds in the various models vary significantly in space and do not correspond to the speeds of isolated waves. The reason, as explained earlier, is obvious. From an oceanic point of view, the low-frequency fluctuations of the surface winds excite a host of waves that give rise to complex phase patterns. The use of terms such as oceanic Kelvin waves in describing low-frequency coupled ocean–atmosphere fluctuations should be regarded as a poetic metaphor. The delay time τ in the delayed oscillator equation should be interpreted as the "memory" of the ocean. It is a measure of the extent to which the ocean is in disequilibrium with the winds at a given time. Once a value for τ has been determined, the period of the Southern Oscillation has been explained. This, however, is a circular argument because τ determines the period of the oscillations and also depends on the period of the oscillation. For example, at extremely long periods τ is practically zero because the ocean has no memory and its response is in equilibrium with the winds. (In this limit the delayed oscillator equation has nonoscillatory, only steady solutions.) As the period of the oscillation decreases the value of τ increases. The delayed oscillator equation is clearly of limited value as an analog of the Southern Oscillation. Its principal flaw is the absence of explicit spatial dependence so that it does not represent an eigenvalue problem. The Southern Oscillation presumably corresponds to the most unstable of a spectrum of coupled ocean–atmosphere modes. The existence of oceanic coasts is likely to result in a discrete set of modes, each with a characteristic spatial structure. [Thus far, stability analyses, such as those of Battisti and Hirst (1989) and Cane et al. (1990), focus on changes in the most unstable mode when there is a change in external parameters—the strength of the ocean–atmosphere coupling, for example. Presumably there are several unstable modes for sufficiently strong coupling.] To regard the delayed oscillator equation as an analog of ocean–atmosphere interactions, it is necessary to assign to the delay time τ a range of values, each of which corresponds to a different spatial structure, rather than a fixed value. The value associated with the largest growth rate for unstable modes is the appropriate value to identify with the modes that appear in coupled models such as HR.

Although the HR model and the simpler coupled ocean–atmosphere models mentioned above capture

FIG. 15. Instantaneous maps of anomalous thermocline displacements [as measured by the vertically integrated temperature to a depth of 300 m (in °C m)] at two monthly intervals in year 8 of the simulation. The thermocline is elevated in lightly stippled areas, depressed in heavily stippled areas, relative to the mean conditions in Fig. 2.

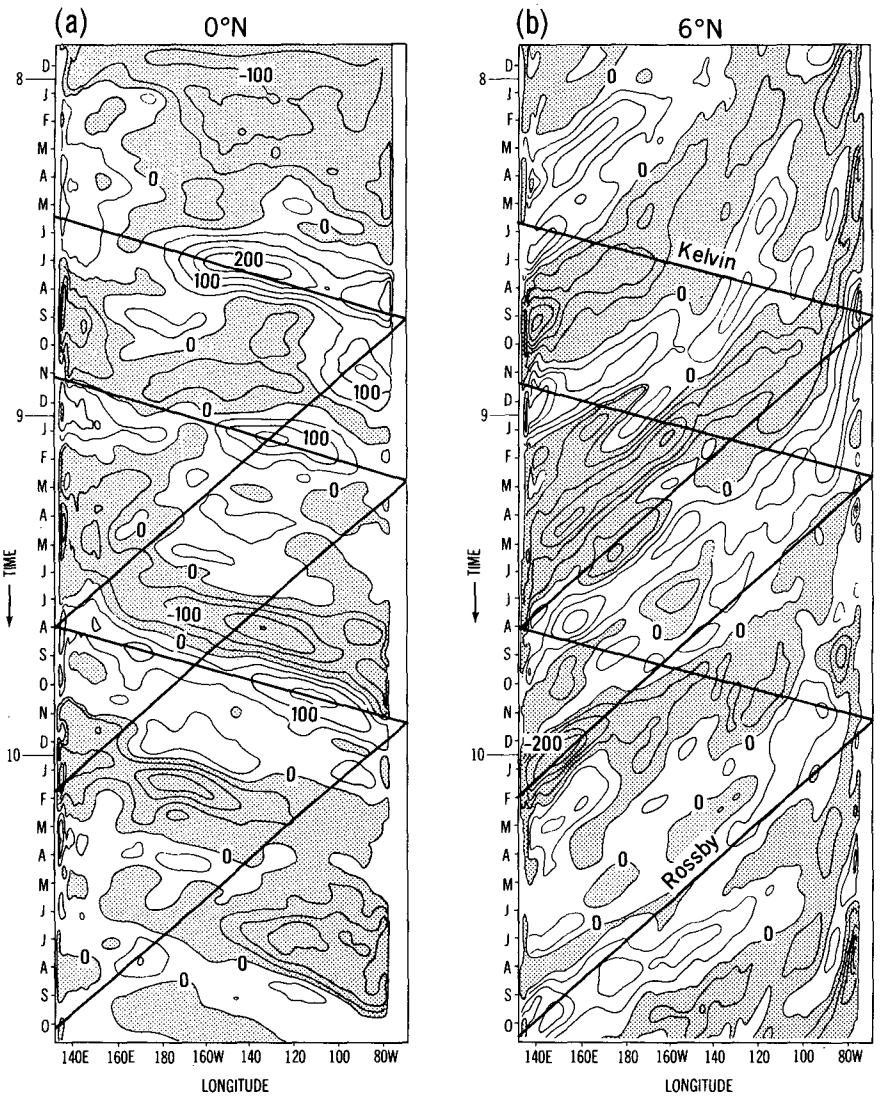

FIG. 16. Variations in the depth of the thermocline [as measured by the vertically integrated temperature to a depth of 300 m (in °C m)] along the equator and along 6°N over a period of 3 years. The data have been bandpass filtered to isolate fluctuations with periods between 2 months and 2 years. The slope of the straight lines indicate the speeds of second baroclinic mode equatorial Kelvin and Rossby modes.

a similar type of ocean–atmosphere mode, there are important differences between the HR model and those other models just cited, especially in the surface wind pattern in response to a sea surface temperature field. In the HR model the westerly winds, during El Niño for example, are displaced farther west relative to the sea surface temperature anomalies and also have a bigger curl so that the off-equatorial elevations of the thermocline in the west are, to a large extent, generated locally in the HR model. These features are evident in Figs. 8, 12, and 14b. In the simpler models referred to above, off-equatorial thermocline elevations in the west arrive there as Rossby waves excited by the wind anomalies farther east. Because these wind anomalies are absent from the far western side of the ocean basin in the simpler models, motion in that region corresponds primarily to free oceanic waves, and there is no superimposed forced motion as in HR. Hence, the change in spatial structure from west to east is not the same as in HR.

Another class of ocean–atmosphere modes exists in which coasts are of secondary importance. These modes, unlike those described thus far, are characterized by phase differences, usually in both time and space, between sea surface temperature and surface wind fluctuations. The LR model captures this type of

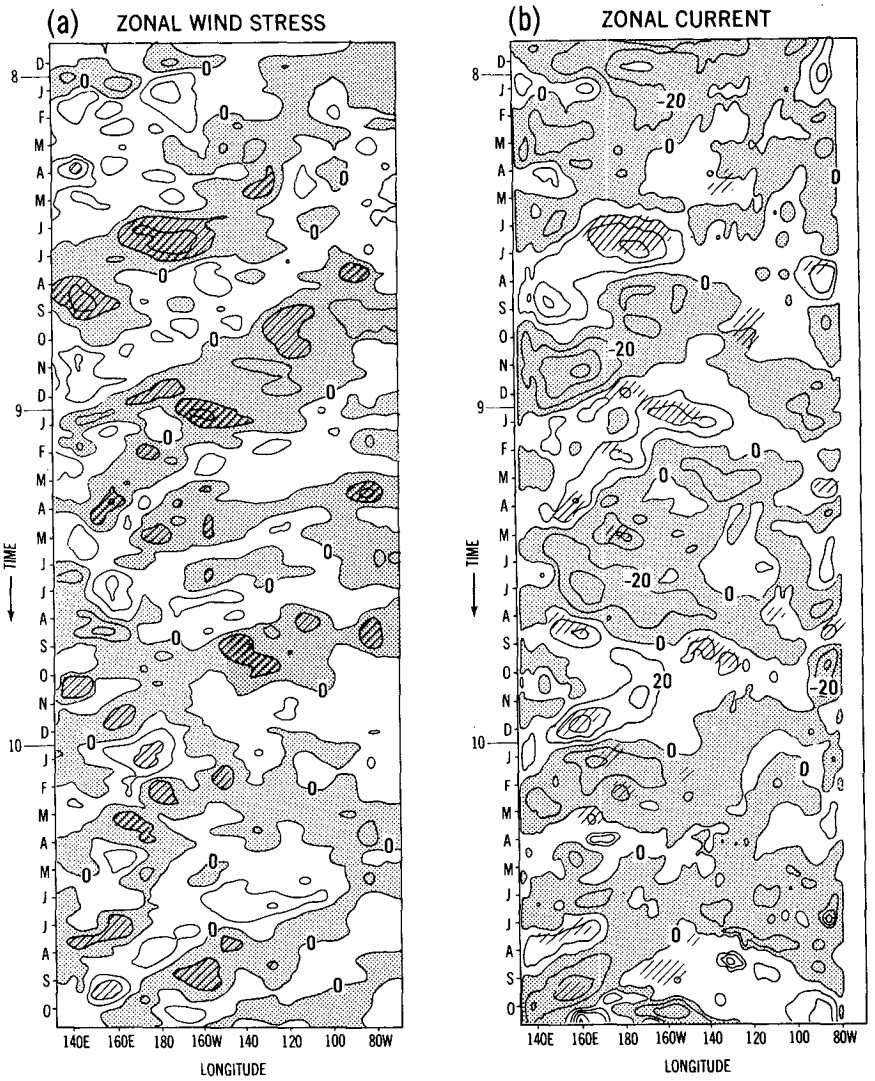

FIG. 17. Variations in the zonal wind stress (left panel) and in the zonal current (right panel) along the equator over the same 3-year period as in Fig. 16. The same filter has been applied to the data. The currents (10^{-2}m s^{-1}) and wind stress (dyn cm^{-2}) are westward in shaded areas. The diagonals, which indicate regions of strong westerly wind anomalies in the left panel, are repeated in the right panel to show how these winds sometimes generate strong currents.

mode, which also appears in the model of Meehl (1990). In the LR model adiabatic changes in sea surface temperature T are primarily due to the following upwelling terms:

$$T_t \approx -\bar{u}T'_x - u'\bar{T}_x - \bar{v}T'_y - v'\bar{T}_y - w'\bar{T}_z,$$

where a bar denotes the time-averaged field. It is demonstrated in Lau et al. (1992) that the contributions from the upwelling term $-w'\bar{T}_z$ are important in the eastern Pacific, whereas the horizontal advection processes tend to dominate in the central and western parts of the basin. If the time t and longitude x dependence is of the form $e^{i(kx+wt)}$, then it follows that the first term on the right results in phase propagation in the direction of $\bar{u}$, which happens to be westward in this model. Because u' is correlated at zero lag with the zonal wind stress τ^x, which is displaced westward of the sea surface temperature anomaly T (see Fig. 15 of Lau et al. 1992), the second term on the right also contributes to westward phase propagation. Analogously, due to the westward shift of the center of meridional divergence in relation to the temperature signal, the term $v'\bar{T}_y$ is also conducive to westward propagation. Hirst (1988) discusses this type of instability that is essentially independent of coasts. Neelin (1991) has recently pointed out that this type of instability is possible even when the dynamic response of the ocean to the winds is an equilibrium one, so that explicit time

dependence disappears from the momentum equations. The time scale of the fluctuations is then longer than both the atmospheric adjustment time to sea surface temperature changes and the dynamic adjustment time of the ocean to wind changes and is controlled by the processes that determine sea surface temperature variations.

The HR and LR models have the same atmospheric component so that the different oceans must be the primary reason why the two models capture different coupled modes. Although sea surface temperatures are calculated globally in the LR model but only in the tropical Pacific in the HR model, the differences in the tropical Pacific probably matter most. In the LR model the sea surface temperature changes in the open ocean, as noted above, are determined primarily locally (see section 6 of Lau et al. 1992). The balance is more complex in the HR model. It is of special interest that the upwelling term $\bar{w}T'_z$ is far more important in HR than LR in determining temperature changes in the upper 50 m of the open ocean. This means that winds in the west that affect the thermocline in the east by means of equatorial Kelvin waves can readily affect sea surface temperatures in the east in HR. This mechanism is a minor one in the LR model because its coarse grid (4.5° latitude, 3.8° longitude) leads to poor resolution of Kelvin waves and because its high eddy viscosity (2.5×10^5 m^2 s^{-1}) damps these waves severely. It follows that the same sea surface temperature perturbation introduced into the two coupled models initially when each is in a steady, equilibrium state will develop differently. In LR the perturbation will be advected westward, but in HR the winds to the west of the temperature perturbation will be able to affect sea surface temperatures in the east. It is therefore not surprising that El Niño evolves differently in the two models. They have significant differences even though sea surface temperature patterns, at the peaks of El Niño and La Niña episodes, are similar in both models.

Both of the coupled models, HR and LR, reproduce Southern Oscillations with a reasonable time scale between El Niño and La Niña episodes that have realistic features. The same is true of some of the simpler coupled models mentioned before. Not all these models are equally relevant to reality because there are important differences between the various simulations, especially in the manner in which El Niño evolves. (It follows that a model cannot be judged simply on the basis of its sea surface temperature patterns at the peaks of El Niño and La Niña.) Comparisons with measurements will ultimately decide which of the coupled models is the most realistic, but the necessary measurements are unavailable. We do however have results from oceanic models, capable of realistic simulations, that have been forced with observed winds (Kitamura 1990; Latif and Flügel 1991; Chao and Philander 1991). Those results all indicate that the Southern Oscillation has a structure very similar to that of the HR model with, for example, differences between the east and west as in Fig. 14 and spatially inhomogeneous zonal phase propagation as in Fig. 13. Analyses of XBT data from the Pacific show the same results (Latif, private communication, 1991). Hopefully, the international program TOGA will provide measurements for a detailed check of the results from the coupled model.

In summary, the HR model reproduces a Southern Oscillation that is very similar to the one that occurs in the tropical Pacific. Although there is no explicit evidence for ocean Kelvin and Rossby waves on interannual time scales, those waves are very prominent at shorter periods in the model. Evidence of such waves in the ocean does not establish the validity of the delayed oscillator mechanism for the Southern Oscillation. The necessary tests are of a different nature, associated with changes in structure between the western and eastern tropical Pacific.

The atmospheric model used in both HR and LR gives, in response to a realistic sea surface temperature pattern, surface winds that are too weak by approximately 30% to 40%. This represents a climate drift problem even though time series, such as those in Fig. 5, are free of trends. Suppose that either of the coupled models were initiated with realistic oceanic and atmospheric conditions. There will be an immediate drift to surface winds that are much weaker. These winds will fail to drive the specified oceanic circulation, which will also drift to a new state. In other words, the use of the coupled models described here for predictions is premature.

Acknowledgments. We are indebted to I. M. Held, J. M. Wallace, K. P. Hamilton, A. H. Oort, and the official reviewers for helpful comments on an earlier version of this manuscript, and to W. Marshall and P. Tunison for expert technical assistance.

REFERENCES

Battisti, D. S., 1988: The dynamics and thermodynamics of a warming event in a coupled tropical atmosphere–ocean model. *J. Atmos. Sci.*, **45**, 2889–2919.

——, and A. C. Hirst, 1989: Interannual variability in the tropical ocean–atmosphere system: Influence of the basic state, ocean geometry and nonlinearity. *J. Atmos. Sci.*, **46**, 1687–1712.

Cane, M. A., and D. W. Moore, 1981: A note on low-frequency equatorial basin modes. *J. Phys. Oceanogr.*, **11**, 1578–1585.

——, and S. E. Zebiak, 1985: A theory for El Niño and the Southern Oscillation. *Science*, **228**, 1085–1087.

——, M. Munnich, and S. Zebiak, 1990: A study of self-excited oscillations of the tropical ocean–atmosphere system. *J. Atmos. Sci.*, **47**, 1562–1577.

Chao, Y., and S. G. H. Philander, 1991: On the structure of the Southern Oscillation. *J. Phys. Oceanogr.*, submitted.

Harrison, D. E., 1989: On climatological monthly mean windstress and windstress curl fields over the World Ocean. *J. Climate*, **2**, 57–70.

Hellerman, S., and M. Rosenstein, 1983: Normal monthly windstress over the World Ocean with error estimates. *J. Phys. Oceanogr.*, **13**, 1093–1104.

Hirst, A. C., 1988: Slow instabilities in tropical ocean basin–global atmosphere models. *J. Atmos. Sci.*, **45**, 830–852.

Kitamura, Y., 1990: Simulation of the annual and interannual variation of the tropical Pacific Ocean. *J. Mar. System*, **1**, 169–181.

Latif, M., and M. Flügel, 1991: An investigation of short range climate predictability in the tropical Pacific. *J. Geophys. Res.*, **96**, 2661–2673.

Lau, N. C., 1985: Modeling the seasonal dependence of the atmospheric responses to observed El Niños 1962–1976. *Mon. Wea. Rev.*, **113**, 1970–1996.

——, and K. M. Lau, 1986: The structure and propagation of intraseasonal oscillations appearing in a GFDL general circulation model. *J. Atmos. Sci.*, **43**, 2023–2047.

——, S. G. H. Philander, and M. J. Nath, 1992: Simulation of ENSO-like phenomena with a low-resolution coupled GCM of the global ocean and atmosphere. *J. Climate*, **5**, 284–307.

Meehl, G. A., 1990: Seasonal cycle forcing of El Niño–Southern Oscillation in a global, coupled ocean–atmosphere GCM. *J. Climate*, **3**, 72–98.

Neelin, J. D., 1991: The slow sea surface temperature mode and the fast-wave limit: Analytic theory for tropical interannual oscillations and experiments in a hybrid coupled model. *J. Atmos. Sci.*, **48**, 584–606.

Pacanowski, R., and S. G. H. Philander, 1981: Parameterization of vertical mixing in numerical models of tropical oceans. *J. Phys. Oceanogr.*, **11**, 1443–1451.

Philander, S. G. H., 1990: *El Niño, La Niña and the Southern Oscillation*, Academic Press, 289 pp.

——, and R. C. Pacanowski, 1981: The response of equatorial oceans to periodic forcing. *J. Geophys. Res.*, **86**, 1903–1916.

——, and A. D. Seigel, 1985: Simulation of El Niño of 1982–83. *Coupled Ocean–Atmosphere Models*, J. Nihoul, Ed., Elsevier, 517–541.

——, D. Halpern, D. Hansen, R. Legeckis, L. Miller, C. Paul, R. Watts, R. Weisberg and M. Winbush, 1985: Long waves in the equatorial Pacific Ocean. *Eos, Trans. Am. Geophys. Union*, **66**, 154.

——, W. Hurlin and A. D. Seigel, 1987: A model of the seasonal cycle in the tropical Pacific Ocean. *J. Phys. Oceanogr.*, **17**, 1986–2002.

Rasmusson, E. M., and T. H. Carpenter, 1982: The relationship between eastern equatorial Pacific sea surface temperatures and summer monsoon rainfall over India and Sri Lanka. *Mon. Wea. Rev.*, **111**, 517–528.

Schopf, P. S., and M. J. Suarez, 1988: Vacillations in a coupled ocean–atmosphere model. *J. Atmos. Sci.*, **45**, 549–566.